IOPscience iopscience.iop.org

Home Search Collections Journals About Contact us My IOPscience

Time-dependent resonant tunnelling for parallel-coupled double quantum dots

This article has been downloaded from IOPscience. Please scroll down to see the full text article.

2004 J. Phys.: Condens. Matter 16 4303

(http://iopscience.iop.org/0953-8984/16/24/012)

View the table of contents for this issue, or go to the journal homepage for more

Download details:
IP Address: 129.252.86.83
The article was downloaded on 27/05/2010 at 15:34

Please note that terms and conditions apply.

INSTITUTE OF PHYSICS PUBLISHING JOURNAL OF PHYSICS: CONDENSED MATTER

J. Phys.: Condens. Matter **16** (2004) 4303–4314 PII: S0953-8984(04)77338-5

Time-dependent resonant tunnelling for parallel-coupled double quantum dots

Bing Dong[1,2], **Ivana Djuric**[1], **H L Cui**[1,3] **and X L Lei**[2]

[1] Department of Physics and Engineering Physics, Stevens Institute of Technology, Hoboken, NJ 07030, USA
[2] Department of Physics, Shanghai Jiaotong University, 1954 Huashan Road, Shanghai 200030, People's Republic of China
[3] School of Optoelectronics Information Science and Technology, Yantai University, Yantai, Shandong, People's Republic of China

Received 2 March 2004
Published 4 June 2004
Online at stacks.iop.org/JPhysCM/16/4303
doi:10.1088/0953-8984/16/24/012

Abstract

We derive the quantum rate equations for an Aharonov–Bohm interferometer with two vertically coupled quantum dots embedded in each of two arms by means of the nonequilibrium Green function in the sequential tunnelling regime. Based on these equations, we investigate time-dependent resonant tunnelling under a small amplitude irradiation and find that the resonant photon-assisted tunnelling peaks in photocurrent demonstrate a combination behaviour of Fano and Lorentzian resonances due to the interference effect between the two pathways in this parallel configuration, which is controllable by threading the magnetic flux inside this device.

1. Introduction

The investigation of quantum coherence in mesoscopic systems has been the subject of considerable interest in solid state physics during recent years. In interference experiments with a quantum dot (QD) embedded in one arm of an Aharonov–Bohm (AB) ring, the tunnelling through a QD was proved to be coherent by detecting the flux-periodic current oscillations [1]. More recently, Holleitner *et al* [2] extended this idea to measure the AB oscillations of the mesoscopic ring containing two coupled QDs inserted in each of the two arms. Furthermore, this parallel-coupled QD structure has been investigated in the Kondo regime, and an observation of the transition between different quantum states has been reported [3, 4]. Clearly, the possibility to manipulate each of the QDs separately and the application of the magnetic flux provide more controllable parameters for designing the transport properties. This has been discussed in several theoretical works for stationary transport by the nonequilibrium Green function (GF) [5–9].

 © 2004 IOP Publishing Ltd Printed in the UK

On the other hand, time-dependent tunnelling through coupled QDs in series has received much attention both theoretically and experimentally. A theoretical study of the photon-assisted tunnelling (PAT) in double QDs given by Stoof and Nazarov [10] and Hazelzet *et al* [11], based on the quantum rate equation approach, predicted that the photoresponse of the system exhibits satellite resonance peaks due to PAT processes which involve the emission or absorption of one photon to match the energy difference between the discrete states of the two QDs. van der Wiel *et al* [12] measured the PAT current through weakly coupled QDs and discovered clearly the predicted extra resonance peaks under microwave irradiation. Motivated by this perfect match between the theory and experiments, we intend, in this paper, to study the PAT in parallel-coupled QDs by the quantum rate equations approach. In this configuration, the additional bridges between the QDs and leads allow the electron wavefunction to propagate along different pathways, then lead to an interference effect between them, which is displayed by the fundamental AB oscillation in the presence of a magnetic field. Therefore, the central point of our study is to explore how the interference influences the photoresponse of the parallel-coupled QDs.

The rest of the paper is organized as follows. First, in the following section, we establish the quantum rate equations for this system in the presence of a magnetic field by employing the nonequilibrium Green function [13, 14][4]. Then in section 3, we calculate the current as a function of magnetic fluxes, and study the quantum dynamics of this system. The spectrum investigation in [9] pointed out that increasing strength of the additional bridges causes the total localization of the antibonding state due to the perfect destructive interference, and as a consequence the transport characteristic of the device reduces approximately to a single QD. In this paper we restrict our interest to the regime where there are two distinctly resolved peaks in the density of states spectra and both the bonding and antibonding states can contribute to transport. Our numerical results show that the current in this regime still keeps the oscillation behaviour with magnetic flux but the period changes from 2π to 4π due to the interdot coupling. The temporal investigation of the electron occupation probabilities in the two QDs shows that the conventional oscillation behaviour in a two-level system can be destroyed by the additional bridges connecting the two QDs and two leads, and it can be recovered by applying a nonzero magnetic flux. Also in this section we study in detail the photoresponse of the system subject to a small irradiation and predict novel enclosed magnetic flux-controlled photon-assisted peaks in tunnelling current, which can be attributed to the interference between the two pathways of electrons going through in this system. Finally, a summary is given in section 4.

2. Model and formulation

We consider the parallel-coupled interacting QD interferometer connected to two normal leads as depicted in figure 1. Only one bare energy level in each dot is involved in transport. The intradot electron–electron Coulomb interactions are assumed to be infinite but the interdot interaction U is finite. Namely, the state of two electrons occupying the same QD is forbidden but two electrons dwelling in different QDs is permitted.

For the sake of simplicity, we abandon the spin because transport through this system is spin independent. Therefore, the available states and the corresponding energies for the interferometer with two embedded QDs are the following:

(1) the whole system is empty, $|0\rangle_1|0\rangle_2$, and the energy is zero;
(2) the first QD is singly occupied, $|1\rangle_1|0\rangle_2$, and the energy is ϵ_1;

[4] Note that this paper gives the temperature- and bias-voltage-dependent quantum rate equations for parallel double QDs without interdot hopping but it is a facile task to include this term in the general rate equations.

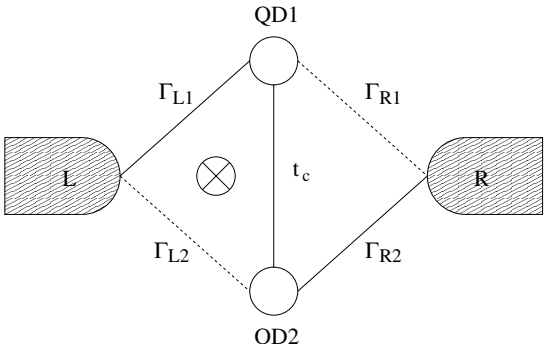

Figure 1. Parallel-coupled quantum dot Aharonov–Bohm interferometer.

(3) the second QD is singly occupied, $|0\rangle_1|1\rangle_2$, and the energy is ϵ_2;
(4) both of the QDs are singly occupied, $|1\rangle_1|1\rangle_2$, and the energy is $\epsilon_1 + \epsilon_2 + U$.

We assign these Dirac brackets as operators: the slave-boson operators $e^\dagger = |0\rangle_1|0\rangle_2$, $d^\dagger = |1\rangle_1|1\rangle_2$ and the pseudo-fermion operators $f_1^\dagger = |1\rangle_1|0\rangle_2$, $f_2^\dagger = |0\rangle_1|1\rangle_2$. Obviously, the explicit (anti)communicators of these auxiliary particles are [13]

$$\begin{aligned} &ee^\dagger = 1, \qquad dd^\dagger = 1, \qquad f_i f_j^\dagger = \delta_{ij}, \\ &ed^\dagger = ef_j^\dagger = f_j e^\dagger = f_j d^\dagger = de^\dagger = df_j^\dagger = 0, \end{aligned} \tag{1}$$

in association with the completeness relation

$$e^\dagger e + d^\dagger d + f_1^\dagger f_1 + f_2^\dagger f_2 = 1. \tag{2}$$

The density matrix elements are expressed as $\rho_{00} = |0\rangle_1|0\rangle_2\,{}_2\langle 0|\,{}_1\langle 0| = e^\dagger e$, $\rho_{11} = |1\rangle_1|0\rangle_2\,{}_2\langle 0|\,{}_1\langle 1| = f_1^\dagger f_1$, $\rho_{22} = |0\rangle_1|1\rangle_2\,{}_2\langle 1|\,{}_1\langle 0| = f_2^\dagger f_2$, $\rho_{dd} = |1\rangle_1|1\rangle_2\,{}_2\langle 1|\,{}_1\langle 1| = d^\dagger d$, and $\rho_{12} = |0\rangle_1|1\rangle_2\,{}_2\langle 0|\,{}_1\langle 1| = f_2^\dagger f_1$. In terms of these slave-particle operators, the Hamiltonian for this system can be written as

$$\begin{aligned} H = &\sum_{\eta,k} \epsilon_{\eta k} c_{\eta k}^\dagger c_{\eta k} + \epsilon_1 f_1^\dagger f_1 + \epsilon_2 f_2^\dagger f_2 + t_c (f_1^\dagger f_2 + f_2^\dagger f_1) + (2\epsilon_d + U) d^\dagger d \\ &+ \sum_k [V_{L1} e^{i\varphi/4} c_{Lk}^\dagger (e^\dagger f_1 + f_2^\dagger d) + \text{H.c.}] \\ &+ \sum_k [V_{L2} e^{-i\varphi/4} c_{Lk}^\dagger (e^\dagger f_2 + f_1^\dagger d) + \text{H.c.}] \\ &+ \sum_k [V_{R1} e^{-i\varphi/4} c_{Rk}^\dagger (e^\dagger f_1 + f_2^\dagger d) + \text{H.c.}] \\ &+ \sum_k [V_{R2} e^{i\varphi/4} c_{Rk}^\dagger (e^\dagger f_2 + f_1^\dagger d) + \text{H.c.}], \end{aligned} \tag{3}$$

where $c_{\eta k}^\dagger$ ($c_{\eta k}$) are the creation (annihilation) operators for electrons with moment k, and energy $\epsilon_{\eta k}$ in lead η ($\eta = L, R$). $V_{\eta j}$ denotes the hopping matrix element between the dot and the lead and $\varphi \equiv 2\pi\Phi/\Phi_0$ accounts for the enclosed magnetic flux inside the AB interferometer ($\Phi_0 = h/e$ is the flux quantum). t_c is the interdot hopping coupling.

We evaluate the statistical expectations of the rate of change of the density matrix elements ρ_{ij} with Hamiltonian (3) and the modified quantization equation (1). After tedious but

straightforward calculations, we obtain

$$\dot{\rho}_{00} = \langle \mathrm{i}[H, e^{\dagger}e]\rangle = \frac{1}{2\pi}\sum_{k}\big\{[\mathbf{V}_e^{\dagger}\mathbf{G}^{<}_{k,e}(t,t)]_{11} - [\mathbf{G}^{<}_{e,k}(t,t)\mathbf{V}_e]_{11} + [\mathbf{V}_e^{\dagger}\mathbf{G}^{<}_{k,e}(t,t)]_{22} - [\mathbf{G}^{<}_{e,k}(t,t)\mathbf{V}_e]_{22}\big\}, \tag{4}$$

$$\dot{\rho}_{ii} = \langle \mathrm{i}[H, f_i^{\dagger}f_i]\rangle = \frac{1}{2\pi}\sum_{k}\big\{[\mathbf{G}^{<}_{e,k}(t,t)\mathbf{V}_e]_{ii} - [\mathbf{V}_e^{\dagger}\mathbf{G}^{<}_{k,e}(t,t)]_{ii} + [\mathbf{V}_d^{\dagger}\mathbf{G}^{<}_{k,d}(t,t)]_{ii} - [\mathbf{G}^{<}_{d,k}(t,t)\mathbf{V}_d]_{ii}\big\} + \mathrm{i}t_{\mathrm{c}}(\rho_{i\bar{i}} - \rho_{\bar{i}i}), \tag{5}$$

$$\dot{\rho}_{dd} = \langle \mathrm{i}[H, d^{\dagger}d]\rangle = \frac{1}{2\pi}\sum_{k}\big\{[\mathbf{G}^{<}_{d,k}(t,t)\mathbf{V}_d]_{11} - [\mathbf{V}_d^{\dagger}\mathbf{G}^{<}_{k,d}(t,t)]_{11} + [\mathbf{G}^{<}_{d,k}(t,t)\mathbf{V}_d]_{22} - [\mathbf{V}_d^{\dagger}\mathbf{G}^{<}_{k,d}(t,t)]_{22}\big\}, \tag{6}$$

$$\dot{\rho}_{12} = \langle \mathrm{i}[H, f_2^{\dagger}f_1]\rangle = \frac{1}{2\pi}\sum_{k}\big\{[\mathbf{G}^{<}_{e,k}(t,t)\mathbf{V}_e]_{12} - [\mathbf{V}_e^{\dagger}\mathbf{G}^{<}_{k,e}(t,t)]_{12} + [\mathbf{V}_d^{\dagger}\mathbf{G}^{<}_{k,d}(t,t)]_{21} - [\mathbf{G}^{<}_{d,k}(t,t)\mathbf{V}_d]_{21}\big\} + \mathrm{i}(\epsilon_2 - \epsilon_1)\rho_{12} + \mathrm{i}t_{\mathrm{c}}(\rho_{11} - \rho_{22}), \tag{7}$$

where the statistical expectations involve the Fourier transformations of the time-diagonal parts of the matrix correlation functions in 2×2 space $[\mathbf{G}^{<}_{e,k}(t,t')]_{ij} \equiv \mathrm{i}\langle c^{\dagger}_{jk}(t')e^{\dagger}(t)f_i(t)\rangle$, $[\mathbf{G}^{<}_{d,k}(t,t')]_{ij} \equiv \mathrm{i}\langle c^{\dagger}_{jk}(t')f_i^{\dagger}(t)d(t)\rangle$, $[\mathbf{G}^{<}_{k,e}(t,t')]_{ij} \equiv \mathrm{i}\langle f_j^{\dagger}(t')e(t')c_{ik}(t)\rangle$, and $[\mathbf{G}^{<}_{k,d}(t,t')]_{ij} \equiv \mathrm{i}\langle d^{\dagger}(t')f_j(t')c_{ik}(t)\rangle$. With the help of the Langreth analytic continuation rules [15], we can relate these hybrid Green functions to the dressed Green functions of the central region:

$$\begin{aligned}\mathbf{G}^{<}_{k,e/d}(t,t') &= \int \mathrm{d}t_1\,[\mathbf{g}^{r}_{k}(t,t_1)\mathbf{V}_{e/d}\mathbf{G}^{<}_{e/d}(t_1,t') + \mathbf{g}^{<}_{k}(t,t_1)\mathbf{V}_{e/d}\mathbf{G}^{a}_{e/d}(t_1,t')],\\ \mathbf{G}^{<}_{e/d,k}(t,t') &= \int \mathrm{d}t_1\,[\mathbf{G}^{r}_{e/d}(t,t_1)\mathbf{V}^{\dagger}_{e/d}\mathbf{g}^{<}_{k}(t_1,t') + \mathbf{G}^{<}_{e/d}(t,t_1)\mathbf{V}^{\dagger}_{e/d}\mathbf{g}^{a}_{k}(t_1,t')],\end{aligned} \tag{8}$$

where $\mathbf{V}_e$ and $\mathbf{V}_d$ are two 2×2 matrixes of the hopping elements defined by

$$\mathbf{V}_e = \begin{pmatrix} V_{L1}\mathrm{e}^{\mathrm{i}\varphi/4} & V_{L2}\mathrm{e}^{-\mathrm{i}\varphi/4}\\ V_{R1}\mathrm{e}^{-\mathrm{i}\varphi/4} & V_{R2}\mathrm{e}^{\mathrm{i}\varphi/4}\end{pmatrix},\qquad \mathbf{V}_d = \begin{pmatrix} V_{L2}\mathrm{e}^{-\mathrm{i}\varphi/4} & V_{L1}\mathrm{e}^{\mathrm{i}\varphi/4}\\ V_{R2}\mathrm{e}^{\mathrm{i}\varphi/4} & V_{R1}\mathrm{e}^{-\mathrm{i}\varphi/4}\end{pmatrix}, \tag{9}$$

and $[\mathbf{g}^{r,a,<,>}_{k}(t,t')]_{ij} = \delta_{ij}g^{r,a,<,>}_{ik}(t,t')$ are the exact Green functions of the ith lead without coupling to the device. These retarded (advanced) and lesser (greater) GFs for the central region are defined as $G^{r(a)}_{oij}(t,t') \equiv \pm\mathrm{i}\theta(\pm t \mp t')\langle\{O_i(t), O_j^{\dagger}(t')\}\rangle$, $G^{<}_{oij}(t,t') \equiv \mathrm{i}\langle O_j^{\dagger}(t')O_i(t)\rangle$, and $G^{>}_{oij}(t,t') \equiv -\mathrm{i}\langle O_i(t)O_j^{\dagger}(t')\rangle$ with $O_j = e^{\dagger}f_j$ if $o = e$ and $O_j = f_j^{\dagger}d$ if $o = d$.

In the following derivation we perform a 'gradient expansion' of equation (8), which is first introduced by Davies *et al* to get the rate equation for resonant tunnelling in the sequential regime [16]. First define centre-of-mass and relative times by $T = (t+t')/2$ and $\bar{t} = (t-t')/2$. Then we assume that functions vary rapidly in the relative time $\bar{t}$ but only slowly in the centre-of-mass time T. Finally, we take a Fourier transform from $\bar{t}$ to ω, and the GF $G(t,t')$ in equation (8) becomes $G(\omega, T)$. According to [16], the lowest-order gradient expansion is a good approximation for sequential resonant tunnelling. Therefore, we just retain the first term in the gradient expansion of the GFs $G(\omega, T)$ in equation (8) and substitute these GFs and the hopping matrixes $\mathbf{V}_{e/d}$ into equations (4)–(7). It is noted that the equal time in equations (4)–(7) means $\bar{t} = 0$ or an integral over all ω. Under the weak coupling (dot–lead tunnelling and interdot hopping) assumption and slowly varying in time T, the GFs in the isolated two-QD system can be expressed in terms of a spectrum representation [13, 14] (see footnote 4).

Inserting these GFs into the Fourier forms of equations (8), we then obtain the final quantum rate equations in the sequential tunnelling regime. Because our interest is focused on studying the quantum dynamics and photoresponse of this interferometer at zero temperature and large bias voltage, we do not intend to give the general expressions but interested readers could refer to our recent paper [14] (see footnote 4). Finally, at zero temperature and large bias voltage, the quantum rate equations are written as

$$\dot{\rho}_{00} = \Gamma_{R1}\rho_{11} + \Gamma_{R2}\rho_{22} - (\Gamma_{L1} + \Gamma_{L2})\rho_{00} + [\Gamma_{R12}\mathrm{e}^{-\mathrm{i}\varphi/2}\rho_{12} + \mathrm{H.c.}], \tag{10}$$

$$\dot{\rho}_{11} = \Gamma_{L1}\rho_{00} + \widetilde{\Gamma}_{R2}\rho_{dd} - (\Gamma_{R1} + \widetilde{\Gamma}_{L2})\rho_{11} + \mathrm{i}t_{\mathrm{c}}(\rho_{12} - \rho_{21}) - [\tfrac{1}{2}(\Gamma_{R12}\mathrm{e}^{-\mathrm{i}\varphi/2} + \widetilde{\Gamma}_{L12}\mathrm{e}^{\mathrm{i}\varphi/2})\rho_{12} + \mathrm{H.c.}], \tag{11}$$

$$\dot{\rho}_{22} = \Gamma_{L2}\rho_{00} + \widetilde{\Gamma}_{R1}\rho_{dd} - (\Gamma_{R2} + \widetilde{\Gamma}_{L1})\rho_{22} + \mathrm{i}t_{\mathrm{c}}(\rho_{21} - \rho_{12}) - [\tfrac{1}{2}(\Gamma_{R12}\mathrm{e}^{-\mathrm{i}\varphi/2} + \widetilde{\Gamma}_{L12}\mathrm{e}^{\mathrm{i}\varphi/2})\rho_{12} + \mathrm{H.c.}], \tag{12}$$

$$\dot{\rho}_{dd} = \widetilde{\Gamma}_{L2}\rho_{11} + \widetilde{\Gamma}_{L1}\rho_{22} - (\widetilde{\Gamma}_{R1} + \widetilde{\Gamma}_{R2})\rho_{dd} + [\widetilde{\Gamma}_{L12}\mathrm{e}^{\mathrm{i}\varphi/2}\rho_{12} + \mathrm{H.c.}], \tag{13}$$

$$\dot{\rho}_{12} = \mathrm{i}(\epsilon_2 - \epsilon_1)\rho_{12} + \mathrm{i}t_{\mathrm{c}}(\rho_{11} - \rho_{22}) + \Gamma_{L12}\mathrm{e}^{-\mathrm{i}\varphi/2}\rho_{00} + \widetilde{\Gamma}_{R12}\mathrm{e}^{\mathrm{i}\varphi/2}\rho_{dd} - \tfrac{1}{2}(\Gamma_{R1} + \Gamma_{R2} + \widetilde{\Gamma}_{L1} + \widetilde{\Gamma}_{L2})\rho_{12} - \tfrac{1}{2}(\Gamma_{R12}\mathrm{e}^{\mathrm{i}\varphi/2} + \widetilde{\Gamma}_{L12}\mathrm{e}^{-\mathrm{i}\varphi/2})(\rho_{11} + \rho_{22}), \tag{14}$$

along with the normalization relation $\rho_{00}+\rho_{11}+\rho_{22}+\rho_{dd} = 1$ due to constraint equation (2) and $\rho_{21} = \rho_{12}^*$, with the definitions $\Gamma_{\eta i} = 2\pi \sum_k |V_{\eta i}|^2\delta(\omega-\epsilon_{\eta k})$ denoting the strength of coupling between the ith QD level and the lead η. Namely, Γ_{Li} (Γ_{Ri}) here describes the tunnelling rate of electrons into (out from) the ith QD when the other QD is empty. In contrast, $\widetilde{\Gamma}_{Li}$ ($\widetilde{\Gamma}_{Ri}$) describes the tunnelling rate of electrons into (out from) the ith QD, when the other QD is already occupied by an electron, revealing the modification of the corresponding rates due to the Coulomb repulsion between the two QDs. The interference in tunnelling events through the different pathways is explicitly described by $\Gamma_{\eta ij}$ and $\widetilde{\Gamma}_{\eta ij}$ for the singly occupied channel and doubly occupied channel, respectively, with the definitions $\Gamma_{\eta ij} = 2\pi \sum_k V_{\eta i}V_{\eta j}\delta(\omega - \epsilon_{\eta k})$. These tunnelling parameters are taken as constant under the wide band limit. In addition, the contribution of the two leads is indeed negative to the nondiagonal density matrix element's dynamic equation, leading to damping of the quantum superposition. It is obvious that these damping terms are different from the series-coupled QDs [10, 11, 19].

Actually, similar equations have already been developed for this system by using other schemes [17, 18]. Jiang and co-workers [17] applied the Gurvitz wavefunction method [19] to derive the modified rate equations and studied the temporary dynamics. However, it should be noted that their equations are different from ours for the nondiagonal density matrix element equation (14). Marquardt and Bruder [18] started from the von Neumann equation of the reduced density matrix and obtained the rate equations at a finite temperature. They studied the dephasing in sequential tunnelling due to electron–phonon interaction for the similar device without interdot hopping. Their equations at zero temperature coincide with ours in the absence of interdot hopping.

The particle current I_η flowing from lead η to the interferometer can be evaluated from the rate of change of the electron number operator $N_\eta(t) = \sum_k c_{\eta k}^\dagger(t)c_{\eta k}(t)$ of lead η [20]:

$$I_\eta(t) = -\frac{e}{\hbar}\left\langle\frac{\mathrm{d}N_\eta}{\mathrm{d}t}\right\rangle = -\mathrm{i}\frac{e}{\hbar}\left\langle\left[H, \sum_k c_{\eta k}^\dagger(t)c_{\eta k}(t)\right]\right\rangle. \tag{15}$$

Ultimately, the current $I_{L/R}$ can be expressed in terms of the GFs:

$$I_{L/R} = \mathrm{i}e\int\frac{\mathrm{d}\omega}{2\pi}\sum_k\left\{\mathbf{G}_{k,e}^<(\omega)\mathbf{V}_e^\dagger - \mathbf{V}_e\mathbf{G}_{e,k}^<(\omega) + \mathbf{G}_{k,d}^<(\omega)\mathbf{V}_d^\dagger - \mathbf{V}_d\mathbf{G}_{d,k}^<(\omega)\right\}_{11/22}. \tag{16}$$

Under the weak coupling approximation, it becomes

$$I_L/e = -(\Gamma_{L1} + \Gamma_{L2})\rho_{00} - \widetilde{\Gamma}_{L2}\rho_{11} - \widetilde{\Gamma}_{L1}\rho_{22} - \widetilde{\Gamma}_{L12}(\mathrm{e}^{\mathrm{i}\varphi/2}\rho_{12} + \mathrm{e}^{-\mathrm{i}\varphi/2}\rho_{21}). \tag{17}$$

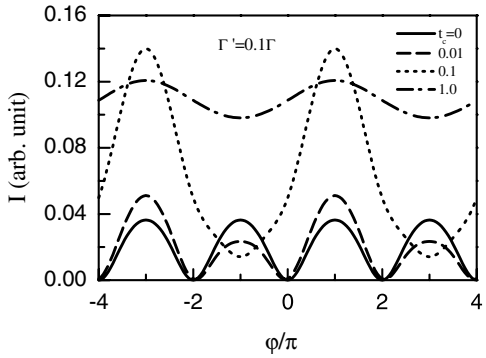

Figure 2. The calculated stationary current I as a function of the magnetic flux φ for different interdot couplings $t = 0, 0.01, 0.1$, and 1 with $\Gamma = 0.2$ and $\Gamma' = 0.1\Gamma$.

The final term in the above expression comes from the contribution of the interference between the upper and lower pathways.

3. Calculations and discussion

3.1. Dc current and quantum dynamics

In this section, we first calculate the current through the parallel-coupled QDs in the presence of magnetic field and then study the quantum dynamical behaviour of this system. The density of states and linear conductance of this system without the Coulomb interaction have been explored in detail in the absence of magnetic flux in the literature [8, 9]. It is found that when the system changes from a configuration in series to a completely symmetrical parallel geometry, the tunnelling through the antibonding state is totally suppressed due to the perfect destructive quantum interference between the different pathways through the system [9]. With this point of view, we limit our investigation to the case of an asymmetric parallel configuration to guarantee that both the bonding and antibonding states have a contribution to the transport, in order to demonstrate the effect of interference on the photoresponse clearly. Here we assume the tunnelling rates $\Gamma_{L1} = \Gamma_{R2} = \widetilde{\Gamma}_{L1} = \widetilde{\Gamma}_{R2} = \Gamma = 0.2$ and $\Gamma_{L2} = \Gamma_{R1} = \widetilde{\Gamma}_{L2} = \widetilde{\Gamma}_{R1} = \Gamma' \leqslant 0.3\Gamma$. Moreover, we have $\Gamma_{L12} = \Gamma_{R12} = \sqrt{\Gamma\Gamma'}$.

Figure 2 displays the stationary current calculated from equation (17) as a function of the renormalized magnetic flux φ for different interdot couplings under the condition $\Gamma' = 0.1\Gamma$. It is clear that in the absence of the interdot coupling, $t_c = 0$, the current I exhibits periodic oscillation with a period of 2π. The current peaks appear at the phases of $(2n + 1)\pi$ (n is an integer number), and the current nearly vanishes at the phases of $2n\pi$. This is the main feature of the conventional AB effect. However, when the interdot coupling turns on, the periodicity of the AB oscillation becomes 4π. In the new AB oscillation pattern, the first current peak also locates at the phase of π. But the positions of the current valleys move from the original phases of 0 and 2π to the phases of $-\pi$ and 3π. A similar characteristic has also been pointed out in [17].

We then study the quantum dynamical behaviour of the system. In calculation, we assume that the system initially occupies the empty state $\rho_{00} = 1$. Figure 3 shows the time evolutions of the electron probability densities ρ_{11} and ρ_{22} for the states $|1\rangle_1|0\rangle_2$ and $|0\rangle_1|1\rangle_2$. In the absence of the interdot hopping $t_c = 0$, the probability ρ_{11} is nearly equal to unity, while ρ_{22} is nearly zero after a long time, because the higher 'injection' rate to the first QD makes electrons occupy this QD, and the higher 'escape' rate of the second QD leads to no electrons staying at

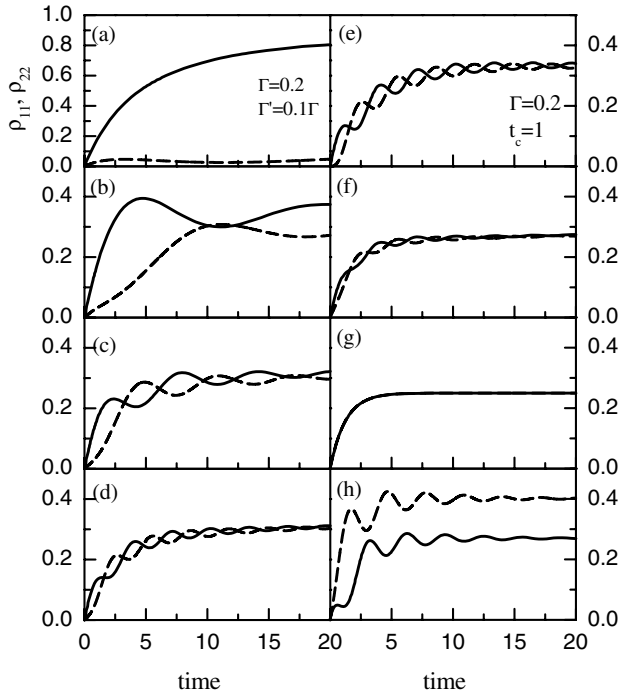

Figure 3. The calculated time evolutions of the electron-occupation probabilities in the two QDs ρ_{11} (solid curves) and ρ_{22} (dashed curves): (a)–(d) different interdot couplings $t_c = 0$, 0.01, 0.1, and 1 with $\Gamma'/\Gamma = 0.1$; (e)–(g) different ratios of the two tunnelling rates $\Gamma'/\Gamma = 0$, 0.5, and 1 with $t_c = 1$; (h) $\Gamma'/\Gamma = 1$ and $\varphi = \pi$. The time unit is $1/5\Gamma$.

all (figure 3(a)). When we turn on the interdot hopping t_c, the probability in the second QD ρ_{22} is greatly enhanced even for very small interdot hopping $t_c = 0.01$ as depicted in figure 3(b). It is also shown that these probabilities display temporal oscillations at small time, meaning that the electron vibrates back and forth between the two QDs. Moreover, the oscillation period is shortened by raising the interdot hopping t_c. This is the well known small t oscillation behaviour in the two-level system: $\rho_{11} \sim \cos^2(t_c t)$ and $\rho_{22} \sim \sin^2(t_c t)$. However, we will find out some new characteristics in this small t oscillation for the parallel-coupled QDs. As indicated in figures 3(d)–(f), the rising tunnelling rate of the additional pathway Γ' gradually destroys the oscillations of the two probabilities due to the increasing quantum interference between the additional pathway and the original one. For equal tunnelling rates of the two pathways, ρ_{11} and ρ_{22} are of course equal and show no oscillations (figure 3(g)). This is a consequence of perfect destructive quantum interference between the different pathways through the parallel-coupled QDs. Furthermore, it is already known that applying the magnetic field will change the scattering phase shift in every QD, and then vary the interference patterns. As a result, the totally vanishing small t oscillations can be recovered to some extent by threading a magnetic flux, which can be observed in figure 3(h) for a normalized magnetic flux $\varphi = \pi$.

3.2. Photoresponse

In this subsection, we study the time-dependent tunnelling through the AB interferometer in the nonlinear regimes. We assume that a time-dependent oscillation signal is applied

to the two interacting QDs, so that the bare energy detuning becomes time dependent, $\epsilon_2 - \epsilon_1 = \epsilon_0 + \delta\cos\Omega t$, where δ is the amplitude and Ω the frequency of the externally applied signal. In the following, we use the approach developed by Stoof and Nazarov [10] to investigate the limiting case of a slight amplitude, $\delta \ll \Omega, \Gamma_{L/R}$, the linear photoresponse.

For simplicity, we assume the interdot Coulomb interaction U is infinite, whereas only one electron can be found inside the system, so $\rho_{dd} = 0$ and all $\widetilde{\Gamma}$ are equal to 0. The quantum rate equations (11)–(14) simplify to

$$\dot{\rho}_{11} = \Gamma\rho_{00} - \Gamma'\rho_{11} + \mathrm{i}t_\mathrm{c}(\rho_{12} - \rho_{21}) - \tfrac{1}{2}[\Gamma_{R12}\mathrm{e}^{-\mathrm{i}\varphi/2}\rho_{12} + \mathrm{H.c.}], \tag{18}$$

$$\dot{\rho}_{22} = \Gamma'\rho_{00} - \Gamma\rho_{22} + \mathrm{i}t_\mathrm{c}(\rho_{21} - \rho_{12}) - \tfrac{1}{2}[\Gamma_{R12}\mathrm{e}^{-\mathrm{i}\varphi/2}\rho_{12} + \mathrm{H.c.}], \tag{19}$$

$$\dot{\rho}_{12} = \mathrm{i}(\epsilon_2 - \epsilon_1)\rho_{12} + \mathrm{i}t_\mathrm{c}(\rho_{11} - \rho_{22}) + \Gamma_{L12}\mathrm{e}^{-\mathrm{i}\varphi/2}\rho_{00} - \tfrac{1}{2}\Gamma_{R12}\mathrm{e}^{\mathrm{i}\varphi/2}(\rho_{11} + \rho_{22}) - \tfrac{1}{2}(\Gamma' + \Gamma)\rho_{12}, \tag{20}$$

with $\rho_{00} + \rho_{11} + \rho_{22} = 1$. Correspondingly, the stationary current simplifies as

$$I_L/e = -(\Gamma + \Gamma')(1 - \rho_{11} - \rho_{22}). \tag{21}$$

We rewrite the simplified quantum rate equations in matrix notation:

$$\frac{\partial\boldsymbol{\rho}}{\partial t} = (\boldsymbol{\Gamma} + \mathbf{T} + \boldsymbol{\epsilon}_0 + \boldsymbol{\delta}\cos\Omega t)\boldsymbol{\rho} + \boldsymbol{c}, \tag{22}$$

where $\boldsymbol{\rho} = (\rho_{11}, \rho_{22}, \rho_{12}, \rho_{21})^\mathrm{T}$, $\boldsymbol{c} = [\Gamma, \Gamma', \Gamma_{L12}\mathrm{e}^{-\mathrm{i}\varphi/2}, \Gamma_{L12}\mathrm{e}^{\mathrm{i}\varphi/2}]^\mathrm{T}$, and $\boldsymbol{\Gamma}$, $\mathbf{T}$, $\boldsymbol{\epsilon}_0$, and $\boldsymbol{\delta}$ are the matrix forms of tunnelling rates, hopping between dots, and time-independent and time-dependent energy differences corresponding to equations (18)–(20). The stationary solution of these equations without irradiation is expressed as

$$\boldsymbol{\rho}^{(0)} = -(\boldsymbol{\Gamma} + \mathbf{T} + \boldsymbol{\epsilon}_0)^{-1}\boldsymbol{c}. \tag{23}$$

Under the condition of small oscillation amplitude, the time-dependent density matrix elements can be expanded as

$$\boldsymbol{\rho} = \boldsymbol{\rho}^{(0)} + \boldsymbol{\rho}^{(1+)}\mathrm{e}^{\mathrm{i}\Omega t} + \boldsymbol{\rho}^{(1-)}\mathrm{e}^{-\mathrm{i}\Omega t} + \boldsymbol{\rho}^{(2)}, \tag{24}$$

where $\boldsymbol{\rho}^{(1\pm)}$ and $\boldsymbol{\rho}^{(2)}$ are the positive (negative) frequency part of the first order correction and frequency-independent second order correction to the stationary solution $\boldsymbol{\rho}^{(0)}$, respectively. They are proportional to the small amplitude of the oscillating signal δ. Substituting the above equation into the time-dependent rate equations and expanding according to the perturbation parameter δ, therefore, we obtain

$$\boldsymbol{\rho}^{(1\pm)} = -\tfrac{1}{2}(\boldsymbol{\Gamma} + \mathbf{T} + \boldsymbol{\epsilon}_0 \mp \mathrm{i}\Omega\boldsymbol{I})^{-1}\boldsymbol{\delta}\boldsymbol{\rho}^{(0)}, \tag{25}$$

$$\boldsymbol{\rho}^{(2)} = -\tfrac{1}{2}(\boldsymbol{\Gamma} + \mathbf{T} + \boldsymbol{\epsilon}_0)^{-1}\boldsymbol{\delta}(\boldsymbol{\rho}^{(1+)} + \boldsymbol{\rho}^{(1-)}), \tag{26}$$

$\boldsymbol{I}$ being the unit matrix. The first order correction $\boldsymbol{\rho}^{(1\pm)}$ provides oscillatory terms and has no contribution to the dc current (time average current) equation (21). The remaining lowest order contribution of the oscillating signal to the dc current comes from the second order correction $\boldsymbol{\rho}^{(2)}$. It is called photocurrent I_ph:

$$I_\mathrm{ph} = (\Gamma + \Gamma')[\boldsymbol{\rho}_{11}^{(2)} + \boldsymbol{\rho}_{22}^{(2)}]. \tag{27}$$

In figure 4 we plot the calculated photoresponse stationary current as a function of ϵ_0 and the irradiation frequency Ω for a given interdot hopping $t_\mathrm{c} = 1$. Figure 4(a) displays the result without the additional pathway $\Gamma' = 0$, which is just the coupled QDs in series. So the characteristic of this figure is the same as figure 2 in [10]:

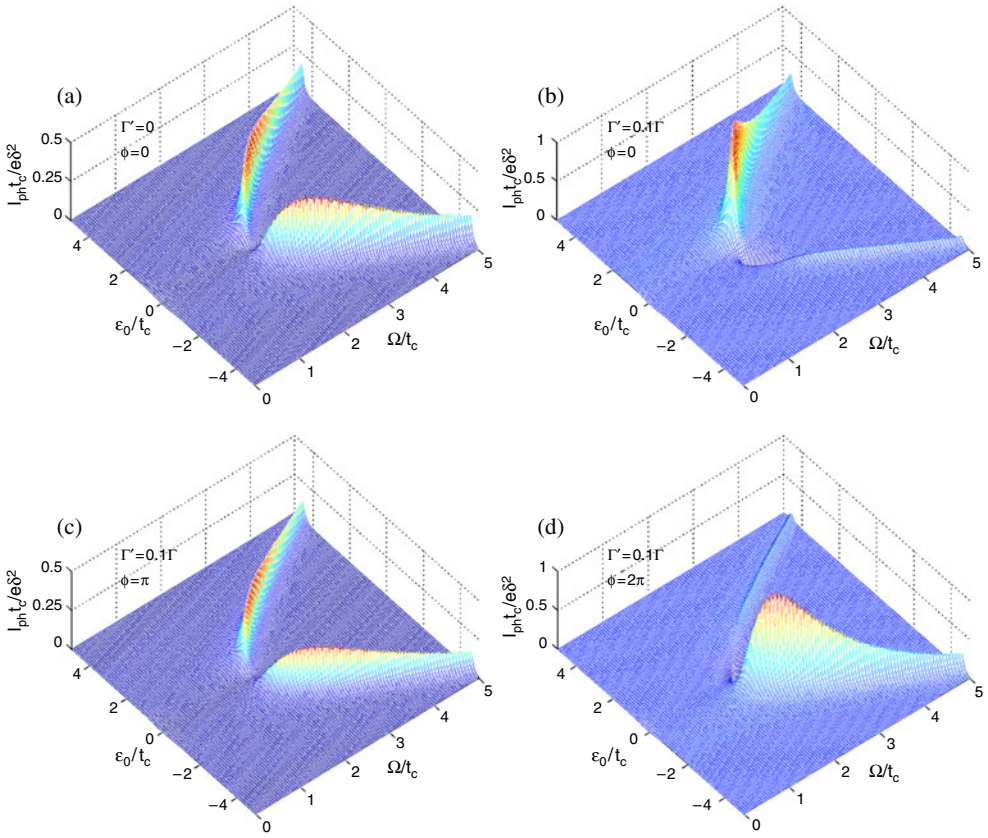

Figure 4. The normalized photocurrent of the parallel-coupled QDs, as a function of the bare level difference ϵ_0/t_c between the two QDs and the frequency Ω/t_c of the irradiation. (a) The rate $\Gamma' = 0$ and the renormalized magnetic flux $\varphi = 0$; (b), (c) $\Gamma'/\Gamma = 0.1$, the magnetic fluxes $\varphi = 0$, π, and 2π.

(This figure is in colour only in the electronic version)

(1) two branches of resonant satellite peaks for ϵ_0 and Ω satisfying $\Omega^2 = \epsilon_0^2 + 4t_c^2$ (positive branch for $\epsilon_0 > 0$, negative branch for $\epsilon_0 < 0$), i.e., resonant PAT occurs when the emission or absorption of one photon can match the renormalized energy difference $\sqrt{\epsilon_0^2 + 4t_c^2}$ of the two levels;
(2) no satellite peak appearance for the case of frequencies below $2t_c$.

This is because the condition of resonant PAT is never satisfied due to the lower energy $\hbar\Omega$ of the applied irradiation. They are the two general conditions for occurrence of the resonant PAT. However, when we switch on the additional pathway with a small rate $\Gamma'/\Gamma = 0.1$, we can observe that the photocurrent behaviour is significantly altered as depicted in figures 4(b) and (c), although the two main characteristics mentioned above keep unchanged. It is clear in figure 4(b) that the positive branch of the PAT peaks is enhanced but the negative branch is suppressed nearly to zero amplitude. We attribute this phenomenon to the interference between the two pathways that electrons can travel through in this new configuration. The scattering phase shifts are different when electrons pass through the two QDs with different bare energy levels. Consequently, the positive energy spacing $\epsilon_0 > 0$ leads to constructive quantum

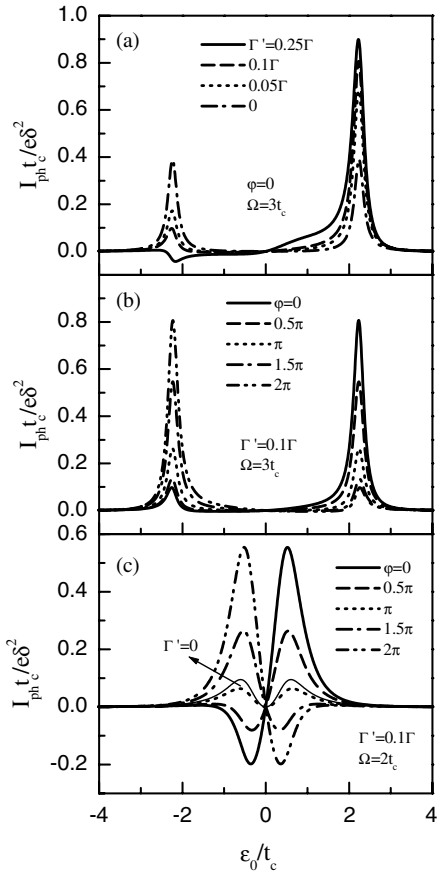

Figure 5. Evolution of the two satellite peaks for different ratios Γ'/Γ and different renormalized magnetic fluxes φ. (a) The plots are for $\Gamma'/\Gamma = 0$, 0.05, 0.1, and 0.25, respectively, at $\varphi = 0$ and $\Omega = 3t_c$; (b) the plots are for $\varphi/\pi = 0$, 0.5, 1.0, 1.5, and 2.0 at $\Gamma'/\Gamma = 0.1$ and $\Omega = 3t_c$; (c) the plots are the same as (b) but for $\Omega = 2t_c$. For the sake of comparison, the result of $\Gamma' = 0$ is denoted as the thin curve in (c).

interference. In contrast, the negative energy difference $\epsilon_0 < 0$ induces destructive quantum interference. This is the reason for the new resonant PAT pattern shown in figure 4(b). This explanation can be further substantiated by the fact that the application of the magnetic fluxes will change the interference fashion, and thus modify the photocurrent behaviour. In figure 4(c) the calculated photocurrent is plotted for a given magnetic flux $\varphi = \pi$. An amazing finding is that the photocurrent becomes very similar to the result of the series-coupled QDs, except with a reduced magnitude. Recalling that the periodicity of the AB oscillation is 4π in the presence of nonzero interdot hopping as pointed out in the above subsection, it is easy to imagine that we will obtain the opposite photoresponse to the situation depicted in figure 4(b) if the renormalized magnetic flux is set to be 2π. The numerical results are plotted in figure 4(d). It is obvious that the negative branch of the resonant PAT peaks rises but the positive one declines.

In the following, we study in detail what actually happens for the reduced satellite peaks in the photoresponse stationary current by analysing the evolution of the resonant PAT peaks as a function of the energy difference ϵ_0 for different ratios of rates Γ'/Γ and renormalized magnetic fluxes φ at a given frequency of the applied irradiation (it must be bigger than or equal to $2t_c$). We plot the calculated results in figure 5. Figure 5(a) is for the frequency of $\Omega = 3t_c$

and several rate ratios in the absence of magnetic field. We can observe more clearly that the two PAT peaks are always located at the points $\epsilon_\pm = \pm\sqrt{\Omega^2 - 4t_c^2}$ irrespective of whether the additional pathway is switched on or not. As the rate of the additional pathway is rising, the peak located at positive position ϵ_+ increasingly heightens and the ϵ_- peak decreases. But the shapes of peaks remain similar to those of $\Gamma' = 0$, in which case the two peaks are entirely identical and have a Lorentzian line shape near the resonance point $\epsilon_\pm$ as revealed in [10], until a stronger rate of the additional pathway $\Gamma'/\Gamma = 0.25$. For this maximum rate considered here, the photocurrent is displayed as a negative dip with very small amplitude instead of a peak. It can be approximated by a Fano line shape. This behaviour has a similar interpretation to those of the linear conductance and density of states when the configuration changes from series to parallel [9]. The interfering of two tunnelling channels opens prominent perspectives for the Fano effect, i.e., asymmetric line shape of the current at the resonant point. In addition, the smaller frequency of irradiation leads to the appearance of the dip in photocurrent more easily (at a smaller rate Γ'). Therefore, the Fano line shape can be observed more clearly at $\Omega = 2t_c$ as shown in figure 5(c).

The effect of the magnetic field on the photoresponse can be clearly observed from figures 5(b) and (c). When the renormalized magnetic flux φ is equal to π, the Fano line shape of the resonant PAT peak completely changes back to the conventional Lorentzian shape if the resonant condition is satisfied. Finally, we conclude that for the moderate ratios of rates Γ'/Γ and frequencies of irradiation, the photoresponse of the considered system expresses itself from the PAT Lorentzian peak to the PAT Fano peak by tuning the magnetic field threaded inside this interferometer.

4. Conclusion

In summary, we have presented the quantum rate equations in the sequential tunnelling regime by means of the nonequilibrium Green function for a mesoscopic AB ring with two tunnelling-coupled QDs embedded in the two arms. Employing this set of quantum rate equations, we calculated the AB oscillation current, the temporal evolution of the electron-occupation probabilities in the two QDs, and the dc photocurrent as the photoresponse in the presence of a weak irradiation, at zero temperature and large bias voltage between the source and the drain.

Our numerical studies show that the permission of hopping between the two dots changes the AB oscillation period to 4π in comparison to the conventional 2π period oscillation observed in the typical AB effect. On the other hand, we find that the small t oscillation of the electron-occupation probabilities is also established in the two QDs, with a damping amplitude controlled by the asymmetry of the parallel configuration. When the configuration is completely symmetrical the small t oscillation is totally destroyed. Interestingly, this oscillation behaviour is reobtained if we vary the enclosed magnetic flux due to the interference effect.

Finally, we have evaluated in detail the dc transport through the parallel-coupled QDs subject to a small external harmonic irradiation. It is found that, as in the series-coupled QDs, the photocurrent of this system exhibits extra resonant peaks when the frequency of the external signal matches the energy difference between the discrete states. Moreover, one branch of the PAT peaks in the photocurrent is enhanced, while another branch is suppressed, which is dependent on the enclosed magnetic flux. This behaviour is a consequence of quantum interference between the different pathways electrons can pass through, and does not exist for series-coupled QDs, where only one pathway exists. For some appropriate rate ratios Γ'/Γ and frequencies of signal Ω, the PAT peaks of photocurrent are composed of Lorentzian and Fano line shapes at the resonant points, respectively, which can also be controlled by applying magnetic fields.

In this paper, we study the time-dependent resonant tunnelling through double QDs in a parallel configuration. This device is receiving wide attention in theoretical and experimental investigations at present, because its tunability makes it suitable for further applications in quantum computation and quantum information. We hope our theoretical results about the novel PAT properties can stimulate experimental studies on this particular problem.

Acknowledgments

BD, ID, and HLC are supported by the DURINT Program administered by the US Army Research Office. XLL is supported by Major Projects of the National Natural Science Foundation of China (10390162 and 90103027), the Special Funds for Major State Basic Research Project (G20000683), and the Shanghai Municipal Commission of Science and Technology (03DJ14003).

References

[1] For review, see Hackenbroich G 2001 *Phys. Rep.* **343** 463
[2] Holleitner A W, Decker C R, Qin H, Eberl K and Blick R H 2001 *Phys. Rev. Lett.* **87** 256802
[3] Holleitner A W, Blick R H, Hüttel A K, Eberl K and Kotthaus J P 2002 *Science* **297** 70
[4] Chen J C, Chang A M and Melloch M R 2003 *Preprint* cond-mat/0305289
[5] Loss D and Sukhorukov E V 2000 *Phys. Rev. Lett.* **84** 1035
[6] König J and Gefen Y 2002 *Phys. Rev.* B **65** 45316
[7] Kubala B and König J 2002 *Phys. Rev.* B **65** 245301
[8] Shahbazyan T V and Raikh M E 1994 *Phys. Rev.* B **49** 17123
[9] Ladrón de Guevara M L, Claro F and Orellana P A 2003 *Phys. Rev.* B **67** 195335
[10] Stoof T H and Nazarov Yu V 1996 *Phys. Rev.* B **53** 1050
[11] Hazelzet B L, Wegewijs M R, Stoof T H and Nazarov Yu V 2001 *Phys. Rev.* B **63** 165313
[12] For review, see van der Wiel W G, De Franceschi S, Elzerman J M, Fujisawa T, Tarucha S and Kouwenhoven L P 2003 *Rev. Mod. Phys.* **75** 1
[13] Dong B, Cui H L and Lei X L 2004 *Phys. Rev.* B **69** 35324
[14] Ma J, Dong B and Lei X L 2003 *Eur. Phys. J.* B **36** 599
[15] Langreth D C 1976 *Linear and Nonlinear Electron Transport in Solids* (*Nato ASI Series B* vol 17) ed J T Devreese and V E Van Doren (New York: Plenum)
[16] Davies J H, Hershfield S, Hyldgaard P and Wilkins J W 1993 *Phys. Rev.* B **47** 4603
[17] Jiang Z T, You J Q, Bain S B and Zheng H Z 2002 *Phys. Rev.* B **66** 205306
[18] Marquardt F and Bruder C 2003 *Preprint* cond-mat/0303397
[19] Gurvitz S A and Prager Ya S 1996 *Phys. Rev.* B **53** 15932
Gurvitz S A 1998 *Phys. Rev.* B **57** 6602
[20] Meir Y and Wingreen N S 1992 *Phys. Rev. Lett.* **68** 2512